BMC Cancer

RESEARCH

Open Access

Exploration of RNA-binding proteins identified RPS27 as a potential regulator associated with Kaposi's sarcoma development

Jingzhan Zhang[1], Peng Wang[2,3,4], Tingting Li[2,3,4], Dong Luo[2,3,4], Yuanyuan Qu[2,3,4], Yuan Ding[2,3,4] and Xiaojing Kang[2,3,4*]

Abstract

Background Kaposi's sarcoma (KS) is a locally aggressive, multicentric tumor. RNA-binding proteins (RBPs) are pivotal for post-transcriptional regulation in various tumors. However, the aberrantly expressed RBP genes and their regulatory patterns in KS remain unclear. This study aimed to identify relevant RBP genes in KS and assess the potential functions and molecular interactions of RPS27, a dysregulated RBP in KS tissues,

Methods Matched KS lesions and normal control tissues from ten patients were chosen for the study. Differentially expressed genes (DEGs) were first identified by RNA-sequencing, and results were validated through an independent public RNA-seq dataset (GSE147704). Among the DEGs, RBPs were selected for further analysis, with RPS27 chosen for detailed investigation due to its dysregulation in KS tissues. RT-qPCR and immunohistochemistry were employed to validate RPS27 expression. Cellular experiments were conducted for dysregulated RPS27 to explore its functions. Additionally, improved RNA immunoprecipitation (iRIP)-seq was performed to investigate potential binding interactions of RPS27 in KS.

Results We identified 828 DEGs through RNA-seq, with 367 overlapping DEGs confirmed by the public RNA-seq dataset. We obtained 48 RBP genes from the overlapping DEGs, including 3 upregulated (*PCBP3, L1TD1*, and *PEG10*) and 45 downregulated RBP genes in KS. Notably, downregulated RBPs included *TECR, PUSL1, DQX1, MAT1A, RACK1*, *EEF1A2,* and *EEF1B2*, and the remaining downregulated RBPs were all ribosomal protein genes, including *RPS27*, which was selected for further exploration. Cellular experiments confirmed that RPS27 inhibition could promote cellular proliferation, migration, invasion, and angiogenesis of HUVECs, consistent with its downregulation in KS. iRIP-seq and RNA-seq analyses showed RPS27's ability to selectively bind to 26 DEGs and showed correlation. The majority of RPS27-bound DEGs were ribosomal protein genes, including *RPL8, RPL13, RPL13A, RPL18, RPL19, RPL23, RPLP1, RPL27A, RPL40, RPS2, RPS4X, RPS13, RPS18, RPS21*, and *RPS27,* which were associated with viral transcription and gene expression.

Conclusion Our results identified dysregulated RBP genes in KS and explored the cellular functions and molecular targets of RPS27, indicating its potential regulatory role in KS development.

Keywords Kaposi's sarcoma, RNA-binding proteins, Ribosomal protein S27, RNA-sequencing, Improved RNA-binding protein immunoprecipitation

*Correspondence:
Xiaojing Kang
kangxiaojing163@163.com
Full list of author information is available at the end of the article

Introduction

Kaposi's sarcoma (KS) is a multifocal, endothelial, proliferative neoplasm of mesenchymal origin [1] and significantly affects patients' quality of life, imposing a substantial economic and psychological burden [2, 3]. It predominantly affects the skin, presenting as purple macules and plaques on both the skin and mucous membranes, and can also infiltrate multiple organs, including internal organs and lymph nodes [4]. In recent years, due to the use of immunosuppressive drugs and HIV infection, the number of KS cases has gradually increased, making it the second most common malignant tumor in HIV-positive patients [5]. Unfortunately, the disease is challenging to treat and prone to relapse [6]. The pathogenesis of KS involves Kaposi's sarcoma-associated herpesvirus (KSHV) infection, immune impairment, and genetic and environmental factors [7]. The application of various omics techniques, including genomics, has accelerated the depth and breadth of research on the immunological underpinnings and molecular mechanisms of tumors. This, in turn, enables precise treatment for susceptible individuals and the development of targeted drugs [8, 9]. Therefore, it is necessary to employ multiple omics approaches to explore the molecular mechanisms underlying the onset and development of KS in depth to identify potential effective targets to guide the diagnosis and treatment of KS.

Among the various omics methods, RNA-sequencing (RNA-seq) is commonly used to characterize the abnormal transcriptome profiles of tumors [10] and has been employed in several KS-associated studies. As early as 2018, Tso et al. sequenced KS tissue and found significant differences in genes related to lipid and glucose metabolism pathways [11]. Subsequently, Ramaswami et al. compared gene expression variations in skin and gastrointestinal KS lesion tissues, revealing heterogeneity in tumor gene expression in different regions, potentially linked to variations in KSHV infection within distinct tumor microenvironments [12]. Furthermore, Lidenge et al. sequenced tissues from 24 patients with KS, detecting a substantial downregulation of numerous ribosomal protein (RP) genes [13]. Thus, RNA-seq is indispensable for identifying differentially expressed genes (DEGs) that have essential roles in important biological processes, including genes encoding RNA-binding proteins (RBPs) [14].

RBPs directly interact with RNAs, governing tissue-specific gene expression and participating in the post-transcriptional regulation of tumors [15–17]. We reviewed the literature focusing on RBPs in KS. We found only a few studies predominantly centered around RBPs associated with KSHV infection and replication, constituting a pivotal element in KS pathogenesis. Research has unveiled that the ORF57 protein encoded by KSHV safeguards viral transcripts against specific nuclear RNA decay pathways by impeding hMTR4 recruitment [18]. Furthermore, the K8 protein functions as an RBP to govern viral DNA replication [19]. However, expressional alterations and regulatory mechanisms of RBPs within the tumor following viral infection in KS remain obscure.

In our investigation, we employed RNA-seq and bioinformatics analysis, such as differential gene expression and RNA-binding profiles, functional enrichment, and co-expression network analysis, to assess upregulated and downregulated RBP genes between KS lesions and normal control tissues. Among the identified RBPs, the RPS27 gene exhibited significant differential expression, prompting us to evaluate its biological functions through cellular experiments and its RNA partners through improved RNA immunoprecipitation and sequencing (iRIP-seq). This study is the first examination of RBP gene expression in KS and delves into the binding patterns of RBPs within this context. The outcomes of this research can offer novel insights into KS pathogenesis, molecular markers, and potential therapeutic targets. These findings must be substantiated through further experimentation.

Materials and methods

Patients and sample collection

We enrolled ten patients with KS who were admitted to the People's Hospital of Xinjiang Uygur Autonomous Region (Table 1). These patients received confirmation through pathological examination and had not undergone any prior treatment. Matched KS skin lesions and normal control skin tissues were collected and preserved in RNA preservation solution at −80 °C. Local surgery was employed to obtain KS tumor tissue and normal control skin tissue, ensuring a distance greater than 0.5 cm from the cancerous lesion edge. This study was approved by the Institutional Review Board of People's Hospital of Xinjiang Uygur Autonomous Region (Register number: KY2021052633), and all participating patients provided written informed consent. All experiments were performed in accordance with the relevant institutional guidelines and regulations.

RNA-seq preparation and analysis

Total RNA was extracted from the KS lesions and normal control tissues of three patients using TRIzol reagent (Invitrogen, USA) [20]. Following RNA extraction, DNase I was used to digest DNA. RNA quality was assessed by measuring the A260/A280 ratio with a Nanodrop™ One/OneC spectrophotometer (Thermo Fisher Scientific, USA). Electrophoresis (1.5% agarose gel) was conducted to verify RNA integrity. Qualified RNAs were quantified with the Qubit™ RNA Assay kit (Life Technologies,

Table 1 Characteristics of the study subjects

Sample ID	Gender	Age (years)	Duration (months)	HIV	Lesion	Type of lesion	Type of experiment
KS251	Male	54	12	Negative	Hand	Plaque	RNA-Seq
KS252	Male	65	17	Negative	Foot	Plaque	RNA-Seq
KS259	Male	63	5	Negative	Foot	Plaque	RNA-Seq
KST2	Male	66	25	Negative	Leg	Nodule	iRIP-Seq
KS250	Male	74	14	Negative	Foot	Plaque	iRIP-Seq
KS263	Male	63	10	Negative	Leg	Nodule	Immunohistochemistry
KS267	Male	60	12	Negative	Leg	Nodule	Immunohistochemistry
KS268	Male	78	5	Negative	Foot	Plaque	Immunohistochemistry
KS272	Male	47	18	Negative	Hand	Plaque	Immunohistochemistry
KS275	Male	67	16	Negative	Foot	Plaque	Immunohistochemistry

HIV human immunodeficiency virus, *RNA-seq* RNA-sequencing, *iRIP-seq* Improved RNA-Binding Protein Immunoprecipitation sequencing

USA). A library for RNA-seq was generated from 2 μg of total RNA using the KCTM Stranded mRNA Library Prep kit for Illumina (Wuhan Seq Health, China). PCR products corresponding to 200–500 bp were enriched. Quantification and final sequencing were performed with a NovaSeq 6000 sequencer (Illumina, USA) using the PE150 model. RNA-seq raw data cleaning and alignment, differentially expressed gene (DEG) screening ($|\log_2 FC| > 2$ and adjusted P-value < 0.05) by DESeq2 (version 1.42.0) [21], and pathway analysis by KOBAS (version 2.0) [22] were then performed following a previously published protocol [23].

Public data retrieval and RBP expression analysis

We obtained the published KS RNA-seq data GSE147704 [13] from the Sequence Read Archive (SRA) database. We utilized the NCBI SRA tool fastq-dump (version 2.10.8, https://github.com/rvalieris/parallel-fastq-dump) to convert the SRA Run files into fastq format. Subsequently, we trimmed the raw reads to eliminate low-quality bases using the FASTX-Toolkit (version 0.0.13, https://github.com/Debian/fastx-toolkit). The quality of the clean reads was assessed by FastQC (version 0.12.1, http://www.bioinformatics.babraham.ac.uk/projects/fastqc). DEGs in KS lesions compared with normal control tissues were conducted by employing the GEO2R tool of the GEO database [24]. Hierarchical clustering heatmaps were generated to illustrate the expression levels of differentially expressed ribosomal RNA (rRNA) genes from RNA-seq data and GSE147704. We compiled a catalog of 2141 human RBPs from four previously published reports and combined the data [16, 25–27]. The selected genes were analyzed using the online network analysis platform (http://bioinfogp.cnb.csic.es/tools/venny/index.html) based on the following criteria: $|\log_2 FC| > 2$ and adjusted P-value < 0.05.

Reverse transcription qPCR validation of DEGs

We performed reverse transcription and quantitative PCR (RT-qPCR) [28] on the previous three matched KS lesions and normal control tissues to validate the DEGs identified by RNA-seq analysis. RNA was reverse-transcribed into cDNA using M-MLV reverse transcriptase (Vazyme, China). Real-time PCR was conducted with a SYBR Green PCR Reagent kit (Yeasen Biotechnology, China). PCR involved an initial denaturation stage at 95 °C for 10 min, followed by 40 cycles at 95 °C for 15 s and 60 °C for 1 min. Three PCR amplification runs were executed for each sample. The expression levels of all genes were normalized to that of *GAPDH*.

Immunohistochemistry

Five matched KS and normal control tissues were fixed in 4% paraformaldehyde for 24 h, followed by dehydration and embedding in paraffin. Sections of 5 μm thickness were cut using a microtome and mounted on poly-L-lysine-coated slides. The sections were deparaffinized by incubating them in xylene and rehydrated using an alcohol-to-water gradient. Antigen retrieval was performed by heating the slides in an autoclave filled with citrate buffer (pH 6.0) at 100 °C for 5 min. After cooling, the slides were blocked with 10% normal serum to prevent nonspecific binding. RPS27 antibody (Proteintech, USA) was added (1:200), and samples were incubated overnight at 4 °C. On the next day, slides were washed and incubated with secondary antibodies (ZSGB-BIO, China) conjugated with horseradish peroxidase for 30 min. The signal was detected using 3,3'-diaminobenzidine, resulting in a brown stain at the site of the antigen. The slides were counterstained with hematoxylin, dehydrated, cleared, and mounted for microscopic examination. Instructions specified for the RPS27 antibody were

followed, and a qualitative method was used to interpret the results.

Cell culture and transfection

Human umbilical vein endothelial cells (HUVECs) were purchased from iCell Bioscience Inc. (Shanghai, China). HUVECs were normally cultured in HUVEC-specific culture medium (iCell, China) in an incubator at 37 °C in an atmosphere with 5% CO_2. The *RPS27* siRNAs and negative control (NC) sequences were obtained from Sangon Biotech (Shanghai, China). They were transfected into indicated cells using Lipofectamine 8000™ (Beyotime, China) following the manufacturer's instructions. *RPS27* siRNAs -for (5'-CCC AAU UCC UAC UUC AUG GAU TT-3') and *RPS27* siRNAs -rev (5'-AUC CAU GAA GUA GGA AUU GGG TT-3'). siRNA NC -for (5'-UUC UCC GAA CGU GUC ACG UTT-3') and siRNA NC-rev (5'-ACG UGA CAC GUU CGG AGA ATT-3').

The experiment was performed by dividing cells into three groups, each with three replicates. The wild-type (WT) group comprised normal HUVEC cells. The siRNA normal control group (siNC) comprised HUVECs transfected with 0.1 μM *RPS27* siRNA NC. Cells were collected after 48 h following the optimal transfection conditions. The *RPS27* siRNA group: HUVECs were transfected with 0.1 μM *RPS27* siRNA and collected after 48 h following the optimal transfection conditions. Total RNA from HUVECs was extracted using the TRIzol™ Reagent (Ambion, USA). The RNA was then reversely transcribed into cDNAs using the One-Step Reverse Transcription Kit (Biosharp, China). The mRNA levels of RPS27 were quantified by RT-qPCR assay (Biosharp, China). The primer sequence information is as follows: *RPS27*-for (5'-GGATCTCCTTCATCCCTCT-3') and *RPS27*-rev (5'-CTGGGCATTTCACATCCA −3'). RT-qPCR and Western blotting were performed to detect the expression of RPS27 after transfection.

Western blot

EDTA trypsin was used to digest the cells, and RIPA lysis buffer (Solarbio, China) was used to lyse the HUVECs to obtain proteins. Proteins were quantified using the BCA method, 12% SDS polyacrylamide gel electrophoresis (Biosharp, China), 5% BSA blocking (Biofroxx, Germany), and primary antibody RPS27 (Proteintech, USA) overnight at 4 °C. The secondary antibody, Goat Anti-Rabbit IgG (H + L) (Proteintech, USA), was used to incubate samples on a horizontal decolorizing shaker at 25 °C for 1 h. β-actin (Abcam, USA) was used as an internal control to normalize the protein expression.The protein band density was identified using a chemiluminescence system (Liuyi Biotechnology, China).

Cell proliferation

Cells were seeded in a 96-well plate at a density of 5×10^4/well, and a CCK-8 assay (TransGen Biotech, China) was conducted following the manufacturer's protocol. Briefly, 100 μL of 10% CCK-8 solution was added into each well at 0, 24, 48, and 72 h after transfection. Cells were incubated with the CCK-8 reagent for 1 h at 37 °C. The suspension was subsequently removed, and cells were incubated with DMSO for another 10 min in the dark. The absorbance at 450 nm was recorded for analysis.

Cell apoptosis

The culture medium from each group was aspirated from the cell flasks into a centrifuge tube (containing suspended cells that have undergone apoptosis or necrosis). Adherent cells were washed twice with PBS, collected in PBS, digested with trypsin, transferred, and centrifuged at 1000 rpm for 5 min. The supernatant was discarded. The samples were washed twice with pre-cooled PBS, and the supernatant was discarded. Next, 500 μL 1 × Binding Buffer was added to resuspend the cells and passed through a 200-mesh sieve. A single-cell suspension was obtained. Next, 5 μL Annexin V-PE and 110 μL 7-AAD were added to each tube, gently mixed, and allowed to stand at 4 ℃ in the dark for 10 min. Flow cytometric (FACSVerse, BD, USA) detection was performed within 30 min to evaluate the level of cell apoptosis.

Cell cycle analysis

The cells were collected and processed by washing them once with PBS. Next, 500 μL pre-cooled PBS was used to resuspend the cells. The cell suspension was added to 3.5 mL of pre-cooled 80% ethanol and fixed overnight at 4 ℃. Cells were centrifuged at 2000 rpm for 5 min, and the supernatant was carefully removed. Cells were washed twice with pre-cooled PBS, and the supernatant was discarded. Cells were resuspended in 500 μL PI/RNase Staining Buffer, passed through a 200-mesh nylon sieve, and a single-cell suspension was obtained. Cells were incubated at 4 ℃ in the dark for 30 min. Red fluorescence and light scattering were detected at an excitation wavelength of 488 nm using a flow cytometer (FACSVerse, BD, USA). An analysis software was used for cell DNA content analysis, and light scattering analysis was performed to evaluate cell cycle characteristics.

Transwell assay

Transwell assay (CORNING, USA) was performed to analyze the migration and invasion abilities of HUVECs after transfection. HUVEC cell-specific culture medium was added to the lower chamber of the 24-well plate, and serum-free medium was added to the upper chamber.

Specifically, 4–5 × 10^4 cells were inoculated in each chamber, and the 24-well plate was shaken and incubated for 24–36 h. In brief, 4% paraformaldehyde was added to the lower chamber to fix cells for 20 min. After washing with PBS, cells were stained with 1% crystal violet solution for 30 min. Under the microscope, 3–6 fields were randomly selected for observation and counting. The experiment was repeated thrice. BD Matrigel (Becton Dickinson, USA) was added for the invasion assay. Other experimental procedures were the same as those for the migration assay.

Tube formation assay

Pre-cooled Matrigel (BD, USA) 50 μL was added into a 96-well plate and incubated for 0.5 h at 37 °C. After culturing each group of cells in serum-free HUVEC cell-specific culture medium for 48 h, a cell suspension was prepared, and 50 μL of cell suspension (1 × 10^5 cells) was seeded in the plate coated with Matrigel and incubated for another 12 h. Representative photographs were subsequently captured under the microscope (IX53, OLYMPUS, Japan) after co-culture. Branches of associated tubes were counted and normalized against the mean value of the control group for calculating the tube formation ratio [29].

iRIP-seq analysis

We selected two cases with large tumor tissues for iRIP experiments. Each of the two KS tissue samples was subjected to iRIP-seq analysis separately. Each sample was divided into an immunoprecipitation (IP) group and an input group. The iRIP-seq experimental method was consistent with the procedure specified by Gao et al. [30]. We applied Piranha (version 1.2.1) for peak calling with default parameters [31]. Target genes for IP were determined from these peaks, and the binding motifs of the IP protein were identified using HOMER software (version 3.12) [32]. To categorize the functional domains of peak-associated genes (target genes), we identified enriched Gene Ontology (GO) and Kyoto Encyclopedia of Genes and Genomes (KEGG) pathways as previously described. For clarity regarding the post-transcriptional binding partners of RPS27, an overlap analysis was performed on the DEGs obtained from the RNA-seq and iRIP-seq data. Key genes were verified using RT-qPCR and RIP-PCR [28].

Statistical analysis

Statistical analysis was primarily conducted using R software (v 4.2.3). Data are presented as means ± standard error of the mean (SEM). Statistical difference between the two groups was calculated using Student's t-test. GraphPad Prism 8.0 was used for the statistical analysis of cell experiments. One-way ANOVA was used to compare data between groups. A P-value < 0.05 was considered statistically significant.

Results

DEG screening and pathway analysis

To identify the DEGs in KS lesions compared to NC tissues, we conducted RNA-seq analysis. Six cDNA libraries were constructed and subsequently subjected to paired-end sequencing. After aligning the quality-filtered reads to the human genome, the RNA-seq data provided a robust expression profile for 20,994 genes. Principal Component Analysis (PCA) based on all DEGs demonstrated clear separation between KS and NC samples (Fig. 1A). A total of 828 DEGs were identified in KS lesions compared with NC tissues, with 275 upregulated and 553 downregulated DEGs (Fig. 1B). To validate our sequencing results, we used published RNA-seq data from 24 patients with KS [13] and performed DEG analysis. We finally identified 87 co-upregulated DEGs and 280 co-downregulated DEGs (Fig. 1C). Functional enrichment analysis revealed that the co-upregulated DEGs were associated with processes such as small GTPase-mediated signal transduction, cell adhesion, positive regulation of protein kinase activity, and protein binding, while the co-downregulated DEGs were primarily linked to translation and cytoplasmic translation processes (Fig. 1D, E). Notably, among the upregulated genes, *FLT4*, a lymphangiogenic factor [33], and *CCL21* and *PROX1*, lymphatic endothelial cell regulatory factors [34, 35], were associated with KS development. Their expression levels were validated by RT-qPCR results and were consistent with the RNA-seq results (Fig. 1F). The above results suggest the dysregulation of the transcriptome profile with potential involvement in KS.

Abnormal expression of RBP genes and pathway analysis

The identity and functions of abnormally expressed RBP genes in KS remain unclear. To address this, we cross-referenced the 2141 reported RBPs with the differentially co-expressed genes identified in both the RNA-seq and GSE147704 datasets. Among the upregulated DEGs, three RBP genes, namely *PCBP3*, *L1TD1*, and *PEG10*, were identified. In contrast, among the co-downregulated DEGs, 45 RBP genes were found, and most of the downregulated RBP genes encode RP (Fig. 2A). The downregulated RBP genes were primarily associated with translation and cytoplasmic translation processes (Fig. 2B), consistent with the co-downregulated DEGs (Fig. 1E). To further validate these findings, we performed RT-qPCR analysis on the same three matched patients mentioned previously. Notably, the RT-qPCR results aligned with the sequencing data (Fig. 2C). These

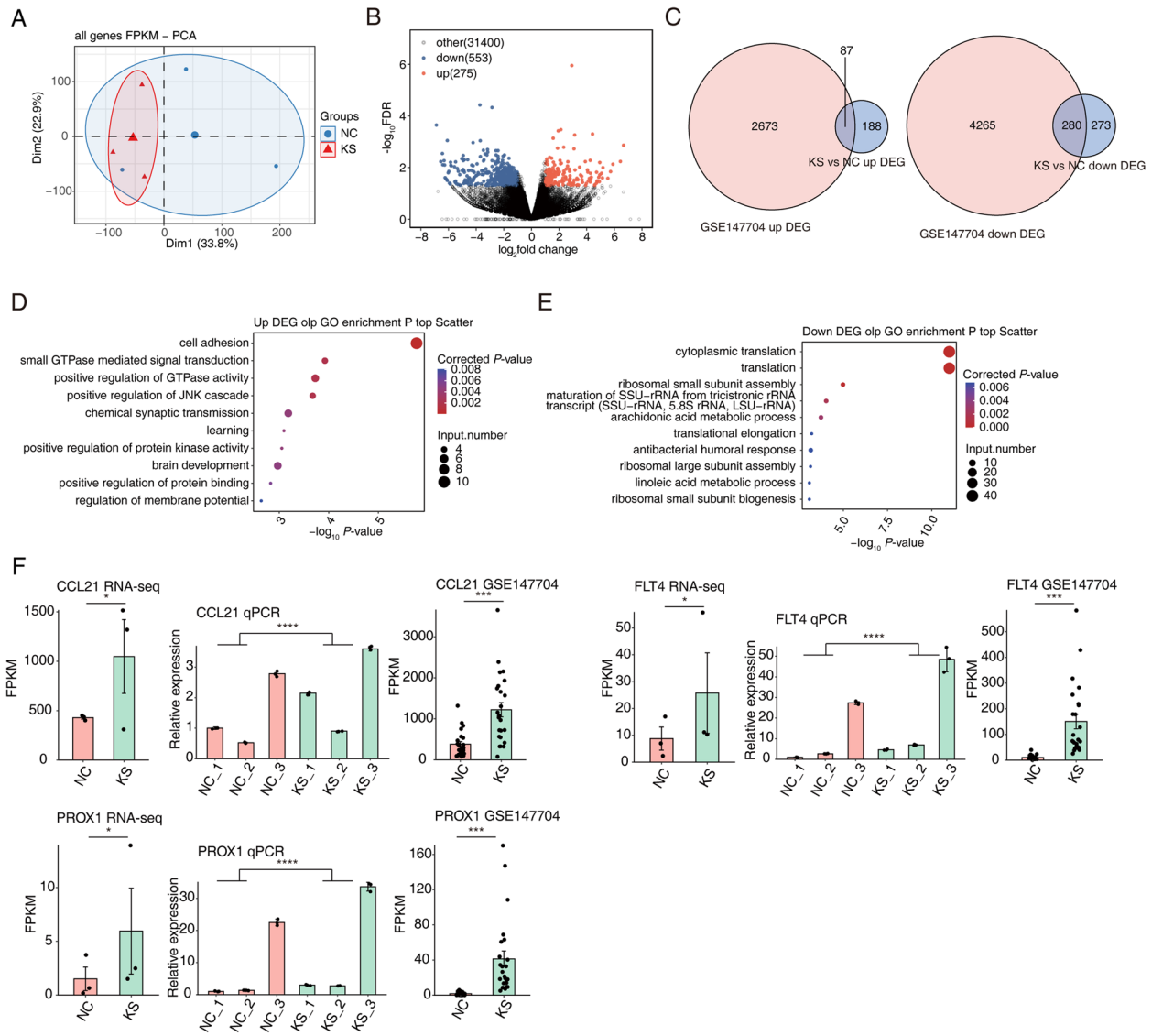

Fig. 1 Differentially expressed genes (DEG) screening and pathway analysis. **A** Principal Component Analysis (PCA) based on the FPKM value of all detected genes. Confidence ellipse in each group. **B** Volcano plot showing the number of DEGs identified in this study. **C** Venn diagram illustrating the co-upregulated DEGs (left panel) and co-downregulated DEGs (right panel) identified in our RNA-seq and GSE147704 data. **D** Bubble chart depicting the most enriched Gene Ontology (GO) biological processes for co-upregulated DEGs. **E** Bubble chart depicting the most enriched GO biological processes for co-downregulated DEGs. **F** Bar graph presenting the expression patterns and statistical differences of DEGs between KS lesions and NC tissues in RNA-seq, GSE147704 data, and RT-qPCR. The error bars indicate the mean ± SEM. * p-value < 0.05, *** p-value < 0.001, **** p-value < 0.0001

results indicate the repression of several RP genes and their potential functions associated with the development of KS. RBPs function through RNA interactions. To delve into the specific RNA targets of RBPs in KS and offer insights for further RBP functional research, we chose to investigate RPS27, a significantly downregulated and validated RBP in KS by RNA-seq and RT-qPCR (Fig. 2C), which is known to be associated with viral infection [36, 37].

Immunohistochemical analysis of RPS27 expression in KS and normal tissues

Immunohistochemical staining was performed to assess RPS27 expression in five pairs of KS tissues and their matched normal tissues, with a focus on endothelial cells. In KS tissues, no expression of RPS27 was detected in the endothelial-cell-derived spindle cells (Fig. 3A-E). However, positive expression of RPS27 was observed in the cytoplasm of endothelial cells (Fig. 3F-J) across all

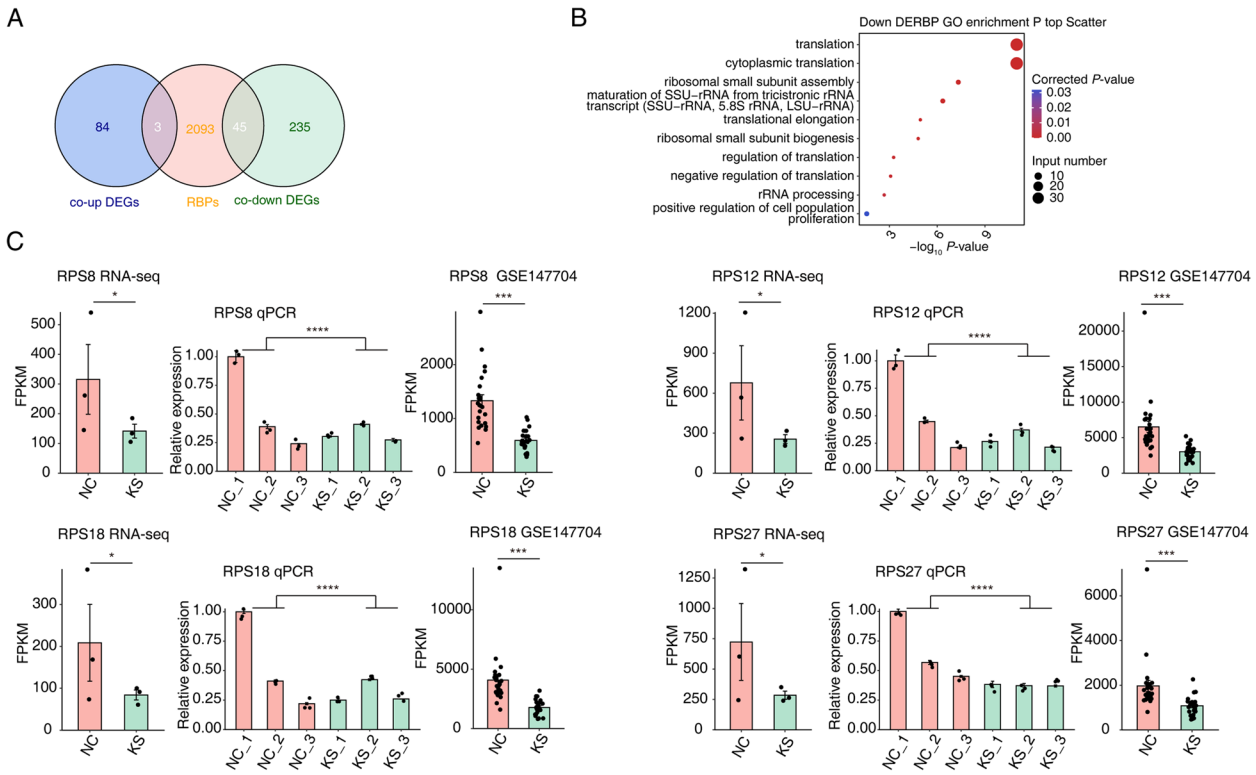

Fig. 2 Abnormally expressed RNA-binding proteins (RBP) genes in Kaposi's sarcoma (KS) lesions compared with normal control (NC) tissues. **A** Venn diagram illustrating the overlap of RBP genes from the reported 2141 RBP genes and the differentially co-expressed genes. **B** Bubble chart displaying the most enriched Gene Ontology (GO) biological processes and Kyoto Encyclopedia of Genes and Genomes (KEGG) for downregulated RBP genes. **C** Bar graph presenting the expression patterns and statistical differences in RBP genes of KS lesions and NC tissues in RNA-seq, GSE147704 data, and RT-qPCR. The error bars indicate the mean ± SEM. *** *p*-value < 0.001, **** *p*-value < 0.0001

five pairs. The results were qualitatively evaluated based on the staining patterns. These observations suggest that RPS27 is expressed at lower levels in the endothelial-cell-derived spindle cells of KS tissues compared to their normal counterparts.

RPS27 inhibition promoted the pro-tumor ability of HUVECs

As KS is an endothelial cell cancer [1], we used HUVECs as the cell model to explore the functions of RPS27. By using siRNAs to silence the expression of RPS27 (siRPS27), we detected a significant decrease in RPS27 expression in both RNA and protein levels compared with WT and negative control (siNC) samples (Fig. 4A, B). By assessing the cell cycle change, a higher percentage of cells were in the G2 phase in siRPS27 samples compared with the other two groups (Fig. 4C). A cell viability experiment also indicated an increased survival rate of HUVECs in siRPS27 samples (Fig. 4D), implying that siRPS27 increased the proliferation ability of HUVECs. There was no significant difference in apoptotic levels among these three groups. Further, we observed that siRPS27 significantly increased the migration and invasion ability of HUVECs (Fig. 4E, F). The ability of tube formation, reflecting angiogenesis and tumorigenesis signatures, was also significantly increased in siRPS27 samples (Fig. 4G). Overall, these results demonstrated the pro-tumor signatures after RPS27 repression in HUVECs, consistent with the downregulation of RPS27 in KS samples.

Identification of RPS27 interacting RNAs in KS tissues

To evaluate how RPS27 interacts with its RNA targets, we conducted an iRIP-seq experiment (Fig. 5A) followed by a comprehensive analysis to uncover RNAs bound by RPS27 in two KS tissues, facilitating the understanding of both direct and indirect RNA-RPS27 interactions. We generated four distinct cDNA libraries, including two replicates for both RPS27_IP and Input samples. After the alignment of iRIP-seq data and peak calling by Piranha, we detected the distribution of peaks across the reference genome. By using the HOMER software, motif analysis of peaks from two RPS27_IP samples revealed the G-rich binding signature of RPS27. Finally, we identified 341 genes associated with RPS27 binding peaks from the results of the two iRIP-seq samples. These genes were

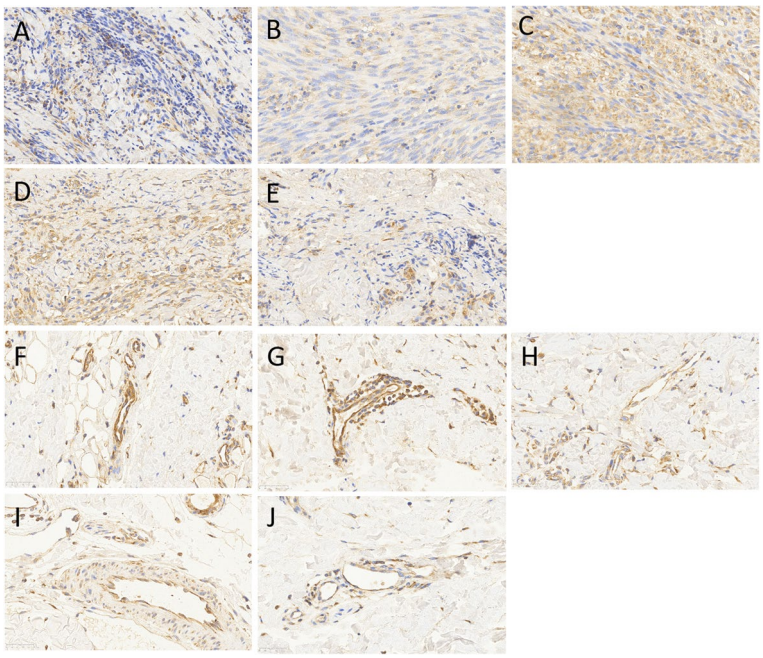

Fig. 3 Immunohistochemical staining for RPS27 in KS and normal tissues. **A-E** No expression is observed in the endothelial-cell-derived spindle cells of KS tissues. **F-J** Representative images show positive expression of RPS27 in the cytoplasm of endothelial cells in normal tissues. A 5-μm scale bar is shown in the lower-left corner of each image

predominantly involved in key pathways, such as translation, SRP-dependent co-translational protein targeting to the membrane, mRNA catabolic process, rRNA processing, and viral transcription (Fig. 5B), indicating that RPS27-bound transcripts have important functions and may affect viral replication in KS tissues. We observed that RPS27 globally bound *EEF1A1*, an important factor controlling translation elongation, and validated their significant interaction by RIP-qPCR experiments (Fig. 5C). RPS27 was bound to the 5'-untranslated regions of WDR74, which is involved in rRNA processing and ribosomal large subunit biogenesis. This interaction was confirmed by RIP-qPCR in both replicates (Fig. 5D). Consistent with the above finding, we propose that RPS27 may have a potential influence on translation or viral transcription by interacting with and affecting transcripts with these functions in KS lesion tissue.

Identification of correlated genes with RPS27 by iRIP-Seq and RNA-seq

To identify the distinct correlated genes with RPS27, we conducted an overlap analysis involving both DEGs by RNA-seq and the 341 RPS27-bound genes. This analysis focused on identifying the expression of dysregulated genes that exhibited potential interaction with RPS27. We identified 26 DEGs that demonstrated this potential interaction (Fig. 6A; p-value = 0.002, hypergeometric test). Among these genes, *TANC2, GRIA1, STOX2, ZFHX3, CNTNAP2, DOCK4, PDE1C, HMBOX1, KIAA1217*, and *PPFIBP1* were upregulated, whereas *RPL8, RPL13, RPL13A, RPL18, RPL19, RPL23, RPLP1, RPL27A, RPL40, RPS2, RPS4X, RPS13, RPS18, RPS21, RPS27*, and *CTH* were downregulated. The downregulated and bound genes were mainly RP genes, indicating that RPS27 prefers to bind to RP transcripts and may modulate their process or translation in KS tissues. Notably, TANC2, a multidomain adapter protein and scaffold protein that interacts with mTOR, has potential relevance in the context of KS treatment [38]. To verify the changed expression and binding potential, we conducted RT-qPCR and RIP-qPCR for *TANC2*, respectively (Fig. 6B, C). The results were consistent with the sequencing data, showing significantly enhanced expression levels and binding signals with RPS27. Furthermore, our GO analysis revealed their collective involvement in various biological processes such as viral transcription, viral gene expression, membrane establishment, protein localization to the endoplasmic reticulum, and SRP-dependent co-translational protein targeting to the membrane. These results further demonstrate that RPS27 is probably involved in translation control and KS development through its interaction with the associated genes and regulation of their expression.

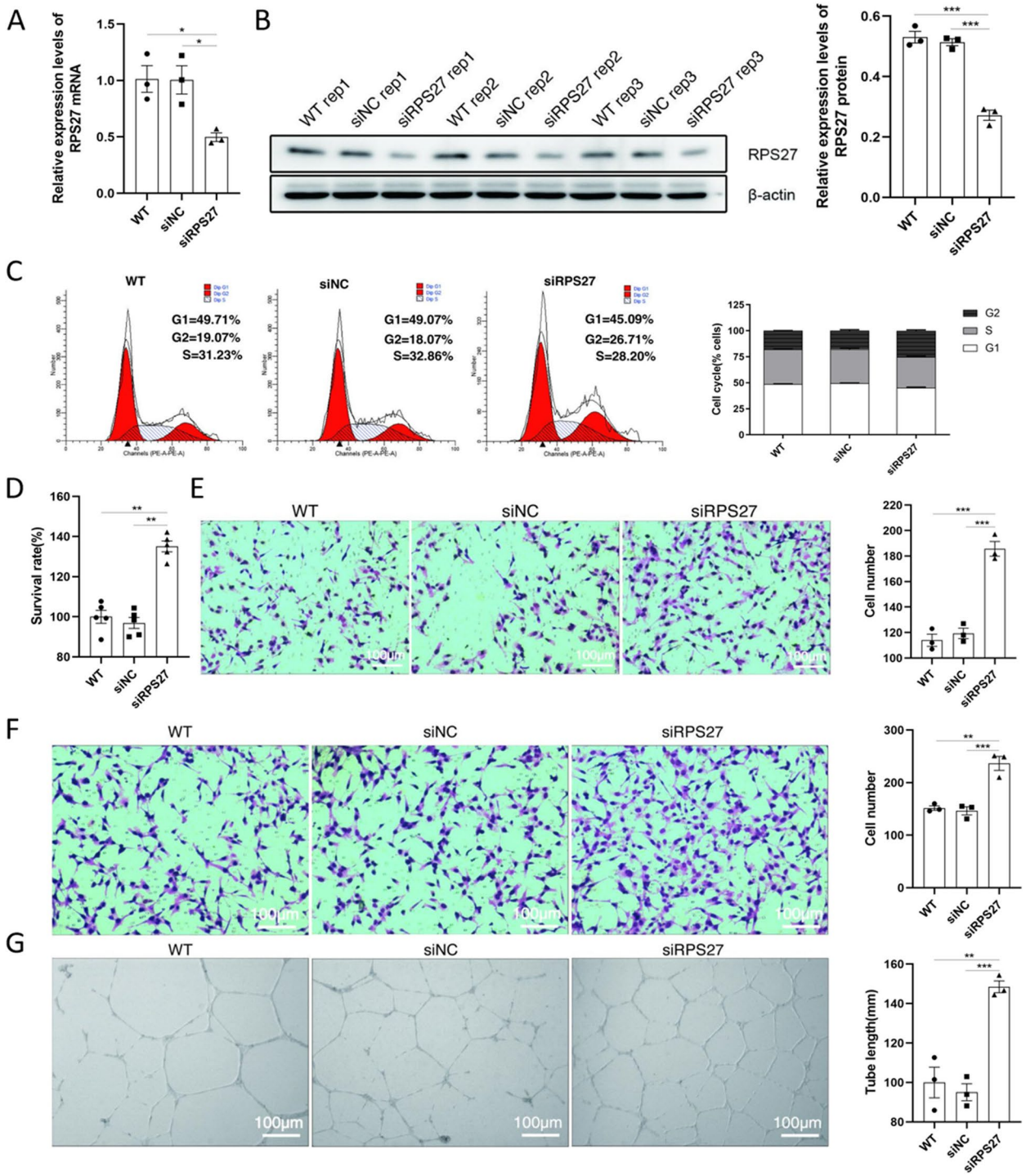

Fig. 4 siRPS27 increased the pro-tumor signatures of HUVECs. **A** Bar plot showing the expression level of RPS27 mRNA in WT, siNC, and siRPS27 samples. **B** Western blot results show the expression level of RPS27 protein in three groups. The right panel shows the quantitative result. **C** Cell cycle results show the percentages of three cellular stages in three groups. The right panel shows the quantitative result. **D** Bar plot showing the cellular proliferation results in three groups. **E** Cell migration results show the migrated cell numbers in three groups. The right panel shows the quantitative result. **F** Cell invasion results show the invaded cell numbers in three groups. The right panel shows the quantitative result. **G** Tube formation results show the tube length in three groups. The right panel shows the quantitative result. * p-value < 0.05; ** p-value < 0.01; *** p-value < 0.001; Student's t-test

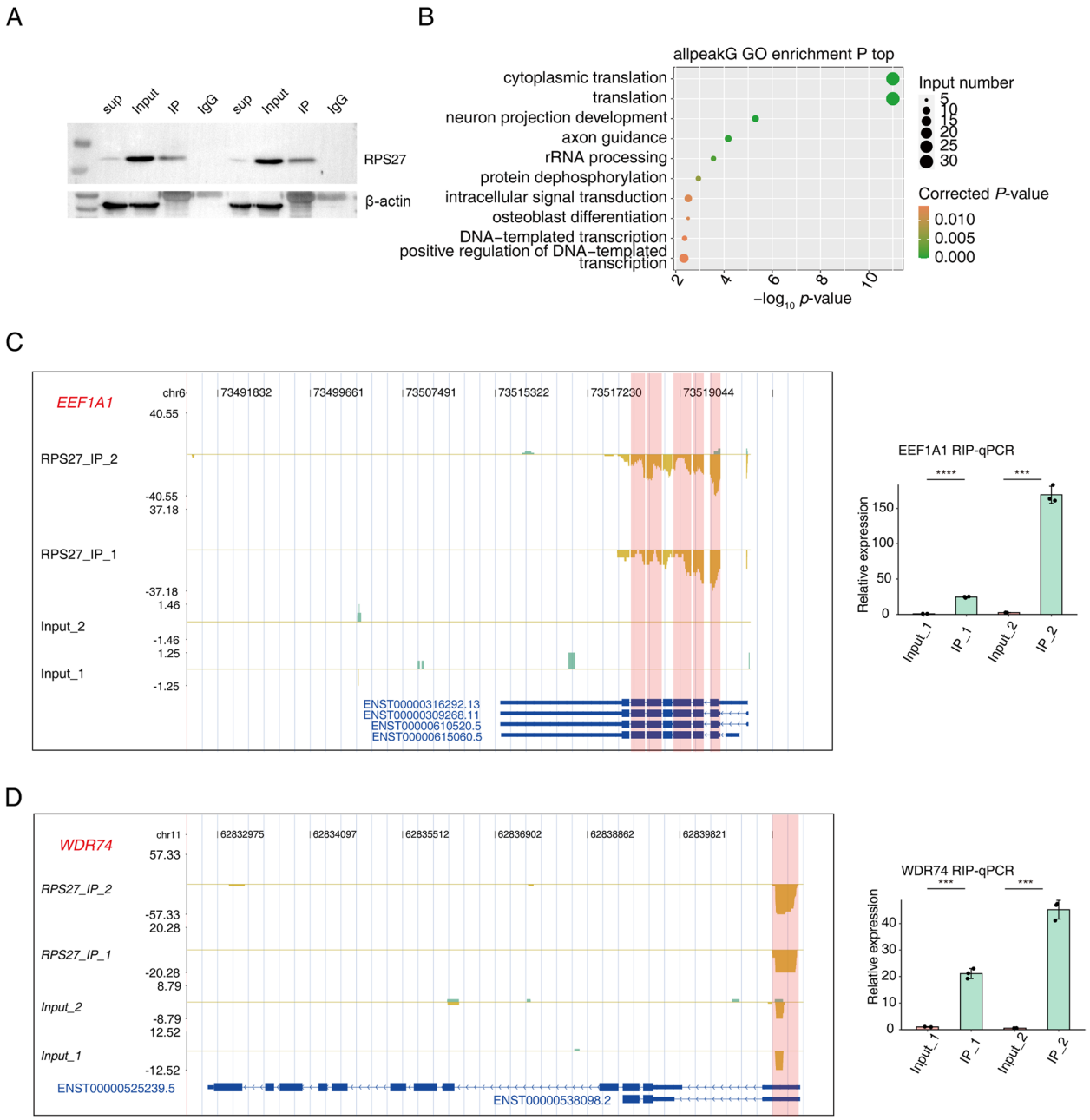

Fig. 5 RPS27 Binding to translation-associated mRNAs in KS tissues. **A** Western blot showing the successful immunoprecipitation of RPS27 in KS tissues. **B** Bubble plot showing the top ten GO BP pathways for RPS27-bound genes. **C** IGV-sashimi plot showing the distribution of *EEF1A1* peak reads in iRIP-seq (left panel). The RIP-qPCR showed the significant binding of RPS27 (right panel). **D** The same as (**C**) but for the binding peaks on *WDR74*. The error bars represent the mean ± SEM. *** *p*-value < 0.001, **** *p*-value < 0.0001, Student's *t*-test

Discussion

In this study, we conducted RNA-seq analysis for KS tissue and subsequently validated the results using the RNA-seq data published by Lidenge et al. [13]. Our analysis unveiled 48 KS-related RBP genes, comprising 3 upregulated and 45 downregulated RBP genes. Among the upregulated RBP genes were *PCBP3, L1TD1,* and *PEG10*. The downregulated genes, except for *TECR, PUSL1, DQX1, MAT1A, RACK1, EEF1A2,* and *EEF1B2,* predominantly belonged to the RP gene category. Specifically, we selected the notably downregulated RP gene *RPS27* in KS tissues for further experiments. Cellular experiments significantly demonstrated the regulatory functions of *RPS27* in tumor development. We

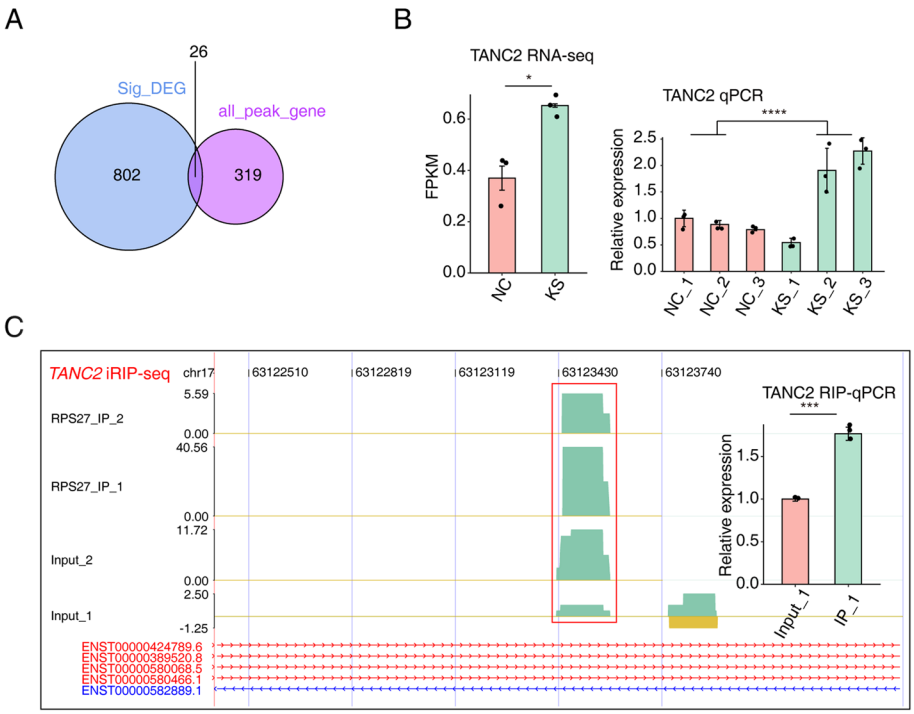

Fig. 6 RPS27 binds to and correlates with translation-associated mRNAs in KS tissues. **A** Venn diagram displaying the overlap between DEGs in RNA-seq and RPS27-bound genes. **B** The bar graph presents the expression patterns and statistical differences of *TANC2* in KS lesions and NC tissues in RNA-seq and RT-qPCR. **C** IGV-sashimi plot showing the distribution of *TNAC2* peak reads in iRIP-seq. The embedded bar graph presents the RPS27-bound abundance and statistical differences of *TNAC2* by RIP-qPCR

employed iRIP-seq to systematically identify its RNA targets and explored its association with DEGs. The RPS27 protein exhibited selective binding to 26 genes. Among them, upregulated genes included *TANC2, GRIA1, STOX2, ZFHX3, CNTNAP2, DOCK4, PDE1C, HMBOX1, KIAA1217*, and *PPFIBP1*. Downregulated genes were mainly ribosomal genes associated with viral transcription and viral gene expression. This observation suggests that distinct RBPs, especially RPS27, may be involved in the pathogenesis and progression of KS, enhancing our comprehension of RBPs in KS pathogenesis and their potential value in KS treatment.

Our findings and those of Lidenge et al. [13] have consistently indicated a substantial downregulation of RP genes in KS lesion tissues. Ribosomes are pivotal protein complexes for cellular protein synthesis. RPs and ribosomal RNAs (rRNAs) work in tandem to translate mRNA into polypeptide chains during protein synthesis. Under normal conditions, cell ribosomes efficiently recognize ribosome binding sites and synthesize proteins. However, viral infections can disrupt this process. Viruses, being small infectious agents with limited genomes, heavily depend on the host cell's structures and functions, which include RPs and rRNA, the primary constituents of ribosomes. Viruses rely on these components to complete their life cycle and generate new viral particles [39, 40]. During this process, the virus may interfere with the functionality and structure of cell ribosomes, thereby affecting their capacity to synthesize proteins. Such alterations can impact normal cellular functions and overall cell survival. Thus, evaluating the translational efficiency change between normal and KS tissues by comparing the polysomes using fractionation or other methods is important in future studies. The downregulation of rRNA expression in KS might be directly related to KSHV through replication modulation. KSHV infection can alter the composition of host cell ribosomes, inducing specific ribosomal populations to facilitate efficient translation of viral mRNAs [41]. Nevertheless, existing antiviral therapies targeting ribosomes involved in viral infections remain limited. Thus, further investigations are warranted to assess antiviral strategies centered on RPs and rRNAs [39].

The expression of *RPS27*, or metallopanstimulin-1, a member of the RPS27E family, was downregulated in KS lesions. RPS27 can activate the NF-κB pathway, thereby regulating the expression of antimicrobial peptides and consequently impeding viral replication [37]. Notably, *RPS27* is associated with various tumors, manifesting as aberrant expression in glioma cells and neurons [42].

Additionally, in the context of cutaneous melanoma, patients with low *RPS27* expression tend to experience poorer prognoses [43]. The protein encoded by *RPS27* encompasses a zinc finger peptide domain, which exhibits an affinity for both zinc and nucleic acids [44, 45]. This zinc finger peptide domain is pivotal in regulating the critical function of *RPS27* in the viral life cycle [36]. RBPs affect cellular proliferation and differentiation by governing the expression of associated proteins. They impact an array of cellular processes, spanning migration, apoptosis, and even angiogenesis, rendering their dysregulation a fundamental mechanism in the onset and progression of cancer [46, 47]. We confirmed that *RPS27* could extensively regulate the cellular processes of HUVECs mentioned above, including cellular proliferation, migration, invasion, and angiogenesis, all of which were tightly associated with the development or progression of tumors. This study unveiled RPS27's capacity to bind to multiple RBP genes, including *EEF1A1* and *WDR74*. The enriched pathways among genes identified as potential binding partners of RPS27 predominantly encompass translation, transmembrane transport, intracellular signal transduction, and SRP-dependent co-translational protein targeting the membrane. Consequently, we ascertained that RPS27 may interact with various RBPs at the transcriptome level, thereby modulating the development of KS.

In transcriptional regulation in KS, *TANC2* emerged as a binding partner for RPS27 and was upregulated in KS. *TANC2* is a multifaceted adapter/scaffold protein that interacts with the mammalian target of rapamycin (mTOR), effectively restraining the signaling pathway. The mTOR signaling system comprises mTORC1 and mTORC2 complexes [48]. Moreover, mTOR signaling exerts considerable influence over the expression of T cell-related cytokines, partaking in immunosuppression, regulating transcription and protein synthesis, and controlling cell growth, apoptosis, and autophagy [49]. Similarly, the administration of rapamycin, an mTOR inhibitor, results in mTOR hyperactivity, as well as synaptic and behavioral irregularities [38]. Rapamycin, functioning as a potent mTORC1 inhibitor and an inducer of autophagy, is a primary therapeutic option for KS [50]. The precise mechanisms underlying the interaction between RPS27 and *TANC2* warrant further investigation, potentially offering novel avenues for targeted treatment in KS. We finally analyzed the functions of correlated genes of RPS27 and found they were enriched in viral development and membrane-associated pathways, indicating that RPS27 may potentially regulate the viral infection and replication that are associated with KS pathogenesis and development.

Despite the identification of dysregulated RBP genes in KS and the selection of *RPS27*, it is evident and credible that various RBPs in KS may interact and collaborate to influence the pathogenesis and progression of this disease. Nevertheless, this study has some limitations. First, the selected RBP genes and their underlying functions necessitate validation within extensive clinical samples. We acknowledge that the choice of RPS27 as a focus for this study is based on its dysregulation in the transcriptome, and its precise role in KS remains to be elucidated. Second, the precise molecular mechanisms through which distinct RBP genes function and interact with one another remain elusive. The role of RBPs in the onset and progression of KS necessitates further evaluation in suitable cell lines and animal models in addition to HUVECs and clinical samples.

Conclusion

In summary, we identified 48 dysregulated RBP genes in KS samples. A significant portion of the downregulated RBP genes comprised ribosomal genes that were probably linked to viral transcription and gene expression. The selected *RPS27* affected the cellular phenotypes of HUVECs that were associated with the development of tumors. We propose that *RPS27* functions probably by interacting with and regulating ribosomal RNAs to modulate translation and viral gene expression. This inference merits verification using additional experiments in the future. Overall, the results suggest a potential synergy of RBPs in the pathogenesis of KS, which expands our comprehension of RBPs in the context of KS and offers valuable insights for further investigation of the disease's underlying mechanisms.

Abbreviations

KS	Kaposi's sarcoma
DEGs	Differentially expressed genes
RBPs	RNA-binding proteins
RNA-seq	RNA-sequencing
iRIP	Improved RNA-Binding Protein Immunoprecipitation
GO	Gene Ontology
KEGG	Kyoto encyclopedia of genes and genomes
KSHV	Kaposi's sarcoma-associated herpesvirus
RT-qPCR	Reverse transcription and quantitative PCR
HUVECs	Human umbilical vein endothelial cells
HIV	Human immunodeficiency virus
RP	Ribosomal protein
rRNA	Ribosomal RNA
mTOR	Mammalian target of rapamycin

Supplementary Information

The online version contains supplementary material available at https://doi.org/10.1186/s12885-025-13790-0.

Supplementary Material 1. The original image of Western blot. Figure 4B showing the expression levels of RPS27 mRNA in WT, siNC, and siRPS27 samples. Figure 5A showing the successful immunoprecipitation of RPS27 in KS tissues

Supplementary Material 2. R codes used in the study. The codes for each section have been separated

Acknowledgements
Not applicable.

Authors' contributions
Jingzhan Zhang and Peng Wang was involved in study design, execution, and manuscript drafting. Tingting Li was involved in study design and acquisition of data. Dong Luo, Yuanyuan Qu, Yuan Ding and Xiaojing Kang contributed to the analysis of data, data evaluation and manuscript preparation. All authors read and approved the final manuscript.

Funding
This study was funded by the Key project of the Natural Science Foundation of Xinjiang Uygur Autonomous Region (2022D01D23) and the National Natural Science Foundation of China (82060502).

Data availability
The RNA-seq data discussed in this article are available from the Gene Expression Omnibus (GEO, http://www.ncbi.nlm.nih.gov/geo/) with the accession number: GSE212962. The data used during the current study are available from the corresponding author on reasonable request.

Declarations

Ethics approval and consent to participate
This study received approval from the Institutional Review Board of People's Hospital of Xinjiang Uygur Autonomous Region (Register number: KY2021052633), and all participating patients provided written informed consent.

Consent for publication
Not applicable.

Competing interests
The authors declare no competing interests.

Author details
[1]Graduate School of Xinjiang Medical University, Urumqi 83001, China. [2]Xinjiang Key Laboratory of Dermatology Research, Urumqi 83001, China. [3]Xinjiang Clinical Research Center for Dermatology and Venereology, Urumqi 83001, China. [4]Department of Dermatology, People's Hospital of Xinjiang Uygur Autonomous Region, Urumqi 83001, China.

Received: 24 October 2024 Accepted: 21 February 2025
Published online: 27 February 2025

References

1. Cesarman E, Damania B, Krown SE, Martin J, Bower M, Whitby D. Kaposi sarcoma. Nat Rev Dis Primers. 2019;5(1):9.
2. Fu L, Tian T, Wang B, Lu Z, Gao Y, Sun Y, Lin YF, Zhang W, Li Y, Zou H. Global patterns and trends in Kaposi sarcoma incidence: a population-based study. Lancet Glob Health. 2023;11(10):e1566–75.
3. Carrilho C, Lunet N. Global trends in Kaposi sarcoma incidence and mortality: the need for action to reduce inequalities. Lancet Glob Health. 2023;11(10): e1479.
4. Addula D, Das CJ, Kundra V. Imaging of Kaposi sarcoma. Abdom Radiol (NY). 2021;46(11):5297–306.
5. Krown SE, Moser CB, MacPhail P, Matining RM, Godfrey C, Caruso SR, Hosseinipour MC, Samaneka W, Nyirenda M, Busakhala NW, et al. Treatment of advanced AIDS-associated Kaposi sarcoma in resource-limited settings: a three-arm, open-label, randomised, non-inferiority trial. Lancet. 2020;395(10231):1195–207.
6. Ngalamika O, Mukasine MC, Kawimbe M, Vally F. Viral and immunological markers of HIV-associated Kaposi sarcoma recurrence. PLoS ONE. 2021;16(7):e0254177.
7. Davis DA, Shrestha P, Yarchoan R. Hypoxia and hypoxia-inducible factors in Kaposi sarcoma-associated herpesvirus infection and disease pathogenesis. J Med Virol. 2023;95(9): e29071.
8. Liu X, Chen W, Zeng Q, Ma B, Li Z, Meng T, Chen J, Yu N, Zhou Z, Long X. Single-Cell RNA-Sequencing Reveals Lineage-Specific Regulatory Changes of Fibroblasts and Vascular Endothelial Cells in Keloids. J Invesy Dermatol. 2022;142(1):124-135 e111.
9. Zhang B, Xie T, Li H, Yi X, Ding M, Xue S, Ji C, Guo H. Targeted gene sequencing reveals disparate genomic mutations between young and older adults in renal cell carcinoma. BMC Cancer. 2024;24(1):1011.
10. Zhang Y, Yao L, Chung CR, Huang Y, Li S, Zhang W, Pang Y, Lee TY. KinPred-RNA-kinase activity inference and cancer type classification using machine learning on RNA-seq data. iScience. 2024;27(4):109333.
11. Tso FY, Kossenkov AV, Lidenge SJ, Ngalamika O, Ngowi JR, Mwaiselage J, Wickramasinghe J, Kwon EH, West JT, Lieberman PM, Wood C. RNA-Seq of Kaposi's sarcoma reveals alterations in glucose and lipid metabolism. PLoS Pathog. 2018;14(1):e1006844.
12. Ramaswami R, Tagawa T, Mahesh G, Serquina A, Koparde V, Lurain K, Dremel S, Li X, Mungale A, Beran A, et al. Transcriptional landscape of Kaposi sarcoma tumors identifies unique immunologic signatures and key determinants of angiogenesis. J Transl Med. 2023;21(1):653.
13. Lidenge SJ, Kossenkov AV, Tso FY, Wickramasinghe J, Privatt SR, Ngalamika O, Ngowi JR, Mwaiselage J, Lieberman PM, West JT, Wood C. Comparative transcriptome analysis of endemic and epidemic Kaposi's sarcoma (KS) lesions and the secondary role of HIV-1 in KS pathogenesis. PLoS Pathog. 2020;16(7):e1008681.
14. Marioni JC, Mason CE, Mane SM, Stephens M, Gilad Y. RNA-seq: an assessment of technical reproducibility and comparison with gene expression arrays. Genome Res. 2008;18(9):1509–17.
15. Van Nostrand EL, Freese P, Pratt GA, Wang X, Wei X, Xiao R, Blue SM, Chen JY, Cody NAL, Dominguez D, et al. A large-scale binding and functional map of human RNA-binding proteins. Nature. 2020;583(7818):711–9.
16. Gerstberger S, Hafner M, Tuschl T. A census of human RNA-binding proteins. Nat Rev Genetics. 2014;15(12):829–45.
17. Cui F, Chen Y, Wu X, Zhao W. Mesenchymal stem cell-derived exosomes carrying miR-486-5p inhibit glycolysis and cell stemness in colorectal cancer by targeting NEK2. BMC Cancer. 2024;24(1):1356.
18. Ruiz JC, Hunter OV, Conrad NK. Kaposi's sarcoma-associated herpesvirus ORF57 protein protects viral transcripts from specific nuclear RNA decay pathways by preventing hMTR4 recruitment. PLoS Pathog. 2019;15(2):e1007596.
19. Liu D, Wang Y, Yuan Y. Kaposi's Sarcoma-Associated Herpesvirus K8 Is an RNA Binding Protein That Regulates Viral DNA Replication in Coordination with a Noncoding RNA. J Virol. 2018;92(7):e02177.
20. Chomczynski P, Sacchi N. Single-step method of RNA isolation by acid guanidinium thiocyanate-phenol-chloroform extraction. Anal Biochem. 1987;162(1):156–9.
21. Love MI, Huber W, Anders S. Moderated estimation of fold change and dispersion for RNA-seq data with DESeq2. Genome Biol. 2014;15(12):550.
22. Xie C, Mao X, Huang J, Ding Y, Wu J, Dong S, Kong L, Gao G, Li CY, Wei L. KOBAS 2.0: a web server for annotation and identification of enriched pathways and diseases. Nucleic Acids Res. 2011;39(Web Server issue):W316-322.
23. Xueqing H, Jun Z, Yueqiang J, Xin L, Liya H, Yuanyuan F, Yuting Z, Hao Z, Hua W, Jian L, Tiejun Y. IGF2BP3 May Contributes to Lung Tumorigenesis by Regulating the Alternative Splicing of PKM. Front Bioeng Biotechnol. 2020;8:679.
24. Davis S, Meltzer PS. GEOquery: a bridge between the Gene Expression Omnibus (GEO) and BioConductor. Bioinformatics. 2007;23(14):1846–7.
25. Castello A, Fischer B, Eichelbaum K, Horos R, Beckmann BM, Strein C, Davey NE, Humphreys DT, Preiss T, Steinmetz LM, et al. Insights into RNA biology from an atlas of mammalian mRNA-binding proteins. Cell. 2012;149(6):1393–406.
26. Castello A, Fischer B, Frese CK, Horos R, Alleaume AM, Foehr S, Curk T, Krijgsveld J, Hentze MW. Comprehensive Identification of RNA-Binding Domains in Human Cells. Mol Cell. 2016;63(4):696–710.
27. Hentze MW, Castello A, Schwarzl T, Preiss T. A brave new world of RNA-binding proteins. Nat Rev Mol Cell Biol. 2018;19(5):327–41.
28. Livak KJ, Schmittgen TD. Analysis of relative gene expression data using real-time quantitative PCR and the 2(-Delta Delta C(T)) Method. Methods. 2001;25(4):402–8.

29. Li B, Liu X, Wu G, Liu J, Cai S, Wang F, Yang C, Liu J. MicroRNA-934 facilitates cell proliferation, migration, invasion and angiogenesis in colorectal cancer by targeting B-cell translocation gene 2. Bioengineered. 2021;12(2):9507–19.
30. Gao C, Chen J, Bai J, Zhang H, Tao Y, Wu S, Li H, Wu H, Shen Q, Yin T. High glucose-upregulated PD-L1 expression through RAS signaling-driven downregulation of PTRH1 leads to suppression of T cell cytotoxic function in tumor environment. J Transl Med. 2023;21(1):461.
31. Uren PJ, Bahrami-Samani E, Burns SC, Qiao M. Site identification in high-throughput RNA–protein interaction data. Bioinformatics. 2012;28:3013.
32. Heinz S, Benner C, Spann N, Bertolino E. Simple Combinations of Lineage-Determining Transcription Factors Prime cis-Regulatory Elements Required for Macrophage and B Cell Identities - ScienceDirect. Mol Cell. 2010;38(4):576–89.
33. Skobe M, Brown LF, Tognazzi K, Ganju RK, Dezube BJ, Alitalo K, Detmar M. Vascular endothelial growth factor-C (VEGF-C) and its receptors KDR and flt-4 are expressed in AIDS-associated Kaposi's sarcoma. J Invest Dermatol. 1999;113(6):1047–53.
34. Choi D, Park E, Kim KE, Jung E, Seong YJ, Zhao L, Madhavan S, Daghlian G, Lee HH, Daghlian PT, et al. The Lymphatic Cell Environment Promotes Kaposi Sarcoma Development by Prox1-Enhanced Productive Lytic Replication of Kaposi Sarcoma Herpes Virus. Can Res. 2020;80(15):3130–44.
35. Sugaya M, Reed S, Rose PP, de la Motte S, Raggo CM, Kurtz SE, Moses AV, Fruh K, Blauvelt A. Kaposi's sarcoma and human dermal microvascular endothelial cells infected with Kaposi's sarcoma-associated herpesvirus express CCL21. J Dermatol Sci. 2011;61(2):139–42.
36. Fernandez-Pol JA. Conservation of multifunctional ribosomal protein metallopanstimulin-1 (RPS27) through complex evolution demonstrates its key role in growth regulation in Archaea, eukaryotic cells, DNA repair, translation and viral replication. Cancer Genom Proteom. 2011;8(3):105–26.
37. Diao MQ, Li C, Xu JD, Zhao XF, Wang JX. RPS27, a sORF-Encoded Polypeptide, Functions Antivirally by Activating the NF-κB Pathway and Interacting With Viral Envelope Proteins in Shrimp. Front Immunol. 2019;10:2763.
38. Kim SG, Lee S, Kim Y, Park J, Woo D, Kim D, Li Y, Shin W, Kang H, Yook C, et al. Tanc2-mediated mTOR inhibition balances mTORC1/2 signaling in the developing mouse brain and human neurons. Nat Comm. 2021;12(1):2695.
39. Li S. Regulation of Ribosomal Proteins on Viral Infection. Cells. 2019;8(5):508.
40. Dong HJ, Zhang R, Kuang Y, Wang XJ. Selective regulation in ribosome biogenesis and protein production for efficient viral translation. Arch Microbiol. 2021;203(3):1021–32.
41. Murphy JC, Harrington EM, Schumann S, Vasconcelos EJR, Mottram TJ, Harper KL, Aspden JL, Whitehouse A. Kaposi's sarcoma-associated herpesvirus induces specialised ribosomes to efficiently translate viral lytic mRNAs. Nat Commun. 2023;14(1):300.
42. Feldheim J, Kessler AF, Schmitt D, Salvador E, Monoranu CM, Feldheim JJ, Ernestus RI, Lohr M, Hagemann C. Ribosomal Protein S27/Metallopanstimulin-1 (RPS27) in Glioma-A New Disease Biomarker? Cancers. 2020;12(5):1085.
43. Floristan A, Morales L, Hanniford D, Martinez C, Castellano-Sanz E, Dolgalev I, Ulloa-Morales A, Vega-Saenz de Miera E, Moran U, Darvishian F, et al. Functional analysis of RPS27 mutations and expression in melanoma. Pigment Cell Melanoma Res. 2020;33(3):466–79.
44. Revenkova E, Masson J, Koncz C, Afsar K, Jakovleva L, Paszkowski J. Involvement of Arabidopsis thaliana ribosomal protein S27 in mRNA degradation triggered by genotoxic stress. EMBO J. 1999;18(2):490–9.
45. Chan YL, Suzuki K, Olvera J, Wool IG. Zinc finger-like motifs in rat ribosomal proteins S27 and S29. Nucleic Acids Res. 1993;21(3):649–55.
46. Wang ZL, Li B, Luo YX, Lin Q, Liu SR, Zhang XQ, Zhou H, Yang JH, Qu LH. Comprehensive Genomic Characterization of RNA-Binding Proteins across Human Cancers. Cell Rep. 2018;22(1):286–98.
47. Kovalski JR, Sarioglu G, Subramanyam V, Hernandez G, Rademaker G, Oses-Prieto JA, Slota M, Mohan N, Yiakis K, Liu I, et al. Functional screen identifies RBM42 as a mediator of oncogenic mRNA translation specificity. Nat Cell Biol. 2025.
48. Mossmann D, Park S, Hall MN. mTOR signalling and cellular metabolism are mutual determinants in cancer. Nat Rev Cancer. 2018;18(12):744–57.
49. Saxton RA, Sabatini DM. mTOR Signaling in Growth, Metabolism, and Disease. Cell. 2017;168(6):960–76.
50. Kerr DA, Busarla SVP, Gimbel DC, Sohani AR, Nazarian RM. mTOR, VEGF, PDGFR, and c-kit signaling pathway activation in Kaposi sarcoma. Human Pathol. 2017;65:157–65.

Publisher's Note